Commun. Comput. Phys.
doi: 10.4208/cicp.OA-2016-0014

Vol. **22**, No. 2, pp. 393-421
August 2017

A Fully Implicit Finite Volume Lattice Boltzmann Method for Turbulent Flows

Fatih Çevik[1,2,*] and Kahraman Albayrak[1]

[1]*Middle East Technical University, Mechanical Engineering Department, Çankaya, Ankara, Turkey.*
[2]*Aselsan Inc., MGEO Division, Unmanned and Autonomous Systems Design Department, Akyurt Ankara, Turkey.*

Communicated by Boo-Cheong Khoo

Received 24 January 2016; Accepted (in revised version) 7 February 2017

Abstract. Almost all schemes existed in the literature to solve the Lattice Boltzmann Equation like *stream & collide, finite difference, finite element, finite volume* schemes are explicit. However, it is known fact that implicit methods utilizes better stability and faster convergence compared to the explicit methods. In this paper, a method named herein as Implicit Finite Volume Lattice Boltzmann Method (IFVLBM) for incompressible laminar and turbulent flows is proposed and it is applied to some 2D benchmark test cases given in the literature. *Alternating Direction Implicit*, an approximate factorization method is used to solve the obtained algebraic system. The proposed method presents a very good agreement for all the validation cases with the literature data. The proposed method shows good stability characteristics, the CFL number is eased. IFVLBM has about 2 times faster convergence rate compared with Implicit-Explicit Runge Kutta method even though it possesses a computational burden from the solution of algebraic systems of equations.

AMS subject classifications: 76M12, 76M28, 76D99, 76F99

Key words: Implicit finite volume, lattice Boltzmann method, turbulent flow.

1 Introduction

There are number of methods to approach an engineering problem that associates with fluid flow. These methods can utilize analytic solutions, empirical formulations, panel methods or computational fluid dynamics (CFD) methods. For the CFD methods, engineers want fast and accurate solutions by solving the discretized governing equations

*Corresponding author. *Email addresses:* cevik.fatih@outlook.com (F. Çevik), albayrak@metu.edu.tr (K. Albayrak)

 ©2017 Global-Science Press

https://doi.org/10.4208/cicp.OA-2016-0014 Published online by Cambridge University Press

of the fluid flows. The CFD methods can be realized by using different types of mathematical solution techniques to solve the Navier Stokes equations and continuity equation which represents the conservation of momentum and mass respectively for isentropic flows. For the last 25 years, scientists and engineers are developing and improving an alternative CFD method that is used to solve the discrete Lattice Boltzmann Equation (LBE) to obtain the macroscopic quantities of the flow field.

The Lattice Boltzmann Method (LBM) has originated from the Lattice Gas Automata method (LGA) [13]. The original implementation of Lattice Boltzmann method has some drawbacks, however it is a powerful alternative to the Navier Stokes equations. The number of researches and published papers on the LBM is increasing year by year, in the CFD community.

Standard Lattice Boltzmann Method has the idea of dealing with particle distributions over a discrete lattice mesh. The LBM can be considered as a simple molecular dynamics model and fills the gap between the microscopic fluid simulations to macroscopic fluid simulations [28]. By simple stream and collide algorithm, particle distributions are calculated for each time advancement. The macroscopic flow quantities are then calculated by using the particle distributions. Since the equations are solved locally, the LBM has a high potential for parallel implementations and has an advantage over other CFD methods. However, the cell size limitations, which is coming from the need of setting Courant Fredrich Lewy number to 1 (CFL=1), exposes an adverse influence on solution time and computational memory requirements. Its simplicity allows a small amount of coding effort while the computational and memory cost for large scale problems are significant. Moreover, the pressure and velocity solutions are not coupled in Lattice Boltzmann Method, which saves computational time compared to NS methods that requires the solution of Poisson's equation for pressure and velocity coupling.

The standard LBM is limited to regular meshes. When bodies with complex boundaries are in focus, the resolution of the mesh is increased to have accurate solutions and that yields increase in computational time and memory requirements. Some alternative techniques are developed to overcome this significant disadvantage of the LBM. The techniques [15, p. 78] can be listed as follows:

- Grid Refinement and Multi-block Methods
- Interpolation Methods
- Finite Difference Lattice Boltzmann Method (FD-LBM)
- Finite Element Lattice Boltzmann Method (FE-LBM)
- Taylor Series Expansion Least Square Based Lattice Boltzmann Method (TS-LBM)
- Finite Volume Lattice Boltzmann Method (FV-LBM)

The first technique is to increase the grid density where large gradients exist. The information exchange takes place according to the set of rules defined by different algorithms.

https://doi.org/10.4208/cicp.OA-2016-0014 Published online by Cambridge University Press

The boundary information can be spread to the flow domain rapidly by coarser grids. The computational cost is reduced significantly by comparing the standard LBM [15]. There are different studies and different algorithms about the application of grid refinement and multi-block technique. Filippova and Hänel [12] are the first to study about the subject. The approach is called FH method and relies on information exchange after the post collision step. The FH method has known instabilities when relaxation parameters of fine or coarse grids are close to unity ($\tau_c \approx 1$ or $\tau_f \approx 1$). Based on the FH method, Dupuis and Chopard [11], develop another method called DC method. Both fine and coarse grid exist at the same time in the solution domain where the refinements are required. The solution information of coarse grid is passed into the fine grid by common grid points. This process has increased the computational efficiency significantly. However the information exchange requires special treatment to overcome the undesired results.

Yu et al. [53] introduced an alternative method that uses grid blocks with different resolutions. The method is called the multi-block method. The solution domain is decomposed into blocks with different grid resolution. Each block is solved by standard LBM and the information exchange is performed on block interfaces. The information exchange method is similar to the one used in FH method. Guo et al. [18] has proposed another domain decomposition method. In this more flexible approach sub-domains may overlap or not. Also the lattice stencil in each domain is not required to be same. The non-equilibrium extrapolation method is used to treat the ghost boundaries of the sub-domains. The information exchange is performed by using the equilibrium distribution functions. The macroscopic quantities (density and velocity) are interpolated from the sub-domains.

The use of adaptive grids are described by Crouse et al. [9]. Their method depends on a sensor variable. The variable itself depends on heuristic approach or derived quantities of the flow to detect the region where a refinement is required. The quantities in the refined cells are calculated by interpolation methods using the parent cells. Crouse's method is generalized by Tölke et al. [45] for multiple relaxation time LBMs. More studies on the subject can be found on Refs. [10, 50, 54].

The second technique that is first proposed by He et al. [22] is known as Interpolation Supplemented LBM (ISLBM). The idea is the computational mesh and the lattice points (where the discrete velocities are set) are separated. Then a calculation process similar to the standard LBM is performed with an additional interpolation step. The ISLBM is still bounded by the CFL=1 condition. Moreover the interpolation schemes needs to be at least second order accurate to minimize the dissipation errors. The second order accurate interpolation schemes do not influence the viscosity of ISLBM. Another advantage of the ISLBM is that the simulated Reynolds number can be increased. That is, a coarser computational mesh can be used for the same level of accuracy with respect to standard LBM for same Reynolds number [23].

The third technique is the Finite Difference Lattice Boltzmann Method. The standard LBM is the upwind finite difference scheme of the Lattice Boltzmann Equation with BGK approximation [3] to the collision operator. Cao et al. [6] first use the finite difference

https://doi.org/10.4208/cicp.OA-2016-0014 Published online by Cambridge University Press

method to discretize the LBE. They used central difference scheme for the spatial derivatives in discrete velocity direction. Moreover a second order explicit Runge Kutta integration scheme is used to advance in time. Mei and Shyy [29] proposed a more general semi implicit scheme applicable to curvilinear coordinate systems. Although the implicit treatment of the collision term has some improvement on stability, the extrapolation used in the equilibrium distribution function has negative impact on the stability. Moreover, the three time step algorithm requires more memory. An alternative semi implicit approach is proposed by Guo and Zhao [16] which does not have the mentioned disadvantages.

The fourth technique is the Finite Element Lattice Boltzmann Method. Lee and Lin [26] proposed the method characteristic Galerkin FE-LBM. Their approach is to integrate the discrete velocity LBE equation along the characteristic line. They used a second order prediction correction method to advance in time. The flow domain is decomposed in to a set of non-overlapping elements [15]. Then the distribution function is projected onto a set of localized piece-wise polynomials associated with the elements. There are different approaches for the FE-LBM, like least squares finite element method [27], and spectral element discontinuous Galerkin method [30].

The fifth technique is called the Taylor Series Expansion and the Least Squares Method (TS-LBM). This method is developed by a group of scientists [7, 34, 41]. In this method the standard LBE goes under Taylor expansion in spatial direction. The expansion is truncated to the second order derivatives. An algebraic set of equations in which the coefficients depends on the coordinates of the grids and lattice velocity is obtained. The method is applicable to different lattice models and reduces to standard LBM for the uniform grids.The unknowns are distribution function and its spatial derivatives to the second order on grid points. The least squares takes place when there is a need solve a overdetermined system [42], which is more grid points are used then the number of unknowns. The application of least square optimizes the error in calculating the unknowns at each grid point.

The final technique is the Finite Volume Lattice Boltzmann Method. The model is developed by Nannelli and Succi. They define a coarse grained distribution function where the standard distribution function is averaged over a control volume [32]. Simple Euler rule is used in time advancement and the flux of distribution function in standard LBM is evaluated from the coarse grained distribution functions by using some interpolation schemes. More advanced alternative finite volume techniques are used later by different researchers [36, 37, 51, 52]. The methods are first order accurate in time. Higher order time advancement scheme as fourth order Runge Kutta method is proposed by Ubertini and Succi [46]. In flux calculation some different methods are used like least squares linear reconstruction method by Stiebler et al. [44] and TVD approach by Patil and Lakshmisha [35]. Guzel and Koc [19] applied Implicit Explicit Runge Kutta (IMEX) [2] method for the FV-LBM and showed the stability is increased with respect to fully explicit schemes. In IMEX scheme for LBM, the characteristic of the collision invariant [47] is used to eliminate the implicit terms, where the time advancement reduces an explicit scheme.

https://doi.org/10.4208/cicp.OA-2016-0014 Published online by Cambridge University Press

All of the above mentioned techniques and methods are either explicit or semi implicit where the implicitness is taken care of by using some methods like extrapolation in time using three time levels or eliminating them by using the properties of LBM. In this manuscript, a fully implicit method is proposed to solve 2D in-compressible turbulent problems on structured non-uniform grids. This method has the same advantages as compared to the other methods associated with non uniform grids. The fine grid near walls will increase the solution accuracy while coarser grids in the flow domain are reducing the calculation burden. Also the method will posses some advantages on stability characteristics as it is an implicit method, and the limitations on the CFL number will be eased. The local time step approach [4, pp. 214-215]is also incorporated with this method.

2 Numerical model

2.1 Discrete Boltzmann equation

The continuous Boltzmann Equation with Bhatnagar-Gross-Krook approximation for the collision term is he starting point of the method presented in this study like many other studies. The continuous Lattice Boltzmann Equation (LBE) is given as:

$$\frac{\partial f}{\partial t}+\vec{e}\cdot\vec{\nabla}f=\Omega(f), \tag{2.1}$$

where f is $(f=f(\vec{x},\vec{e},t))$ the particle density distribution function. The arguments of the distribution function are position vector $(\vec{x})$, particle velocity vector $(\vec{e})$ and time (t). $\Omega(f)$ is the collision operator [3]. The collision operator given in Eq. (2.1) is defined as

$$\Omega(f)=-\frac{1}{\tau_c}(f-f^{eq}). \tag{2.2}$$

In Eq. (2.2), f^{eq} is the equilibrium distribution function (or Maxwell-Boltzmann distribution function), and τ_c is the relaxation time. When we substitute the collision operator to Boltzmann Equation, the following continuous LBE is obtained:

$$\frac{\partial f}{\partial t}+\vec{e}\cdot\vec{\nabla}f=-\frac{1}{\tau_c}(f-f^{eq}). \tag{2.3}$$

Eq. (2.3) can be discretized [15, p. 18] in a set of direction in velocity space where f_α is the density distribution function, e_α is the discrete velocity and f_α^{eq} is the equilibrium distribution function in the α^{th} direction

$$\frac{\partial f_\alpha}{\partial t}+\vec{e_\alpha}\cdot\vec{\nabla}f_\alpha=-\frac{1}{\tau_c}(f_\alpha-f_\alpha^{eq}). \tag{2.4}$$

Since, 2D implementation is presented in this paper, D2Q9 stencil [21] is used for discrete velocity directions. in Fig. 1, the D2Q9 stencil is shown.

https://doi.org/10.4208/cicp.OA-2016-0014 Published online by Cambridge University Press

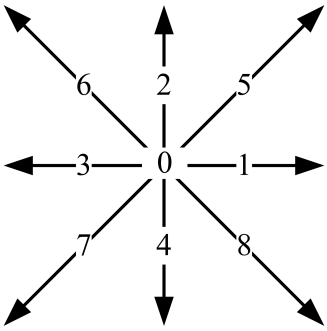


Figure 1: D2Q9 stencil.

The discrete velocities of D2Q9 model are given as:

$$e_{\alpha x,\alpha y}=\begin{cases}0 & \text{for } \alpha=0,\\ c(\cos((\alpha-1)*\pi/2),\sin((\alpha-1)*\pi/2)) & \text{for } \alpha=1,2,3,4,\\ \sqrt{2}c(\cos((\alpha-5)*\pi/2+\pi/4),\sin((\alpha-5)*\pi/2+\pi/4)) & \text{for } \alpha=5,6,7,8,\end{cases} \tag{2.5}$$

where c is a constant and it is related to the speed of sound with the following relation $c=c_s\sqrt{3}$ relation.

The equilibrium distribution functions for D2Q9 model is given as:

$$f_\alpha^{eq}=\rho\omega_\alpha\left[1+3\frac{\vec{e}_\alpha\cdot\vec{u}}{c^2}+\frac{9}{2}\frac{(\vec{e}_\alpha\cdot\vec{u})^2}{c^4}-\frac{3}{2}\frac{(\vec{u})^2}{c^2}\right], \tag{2.6}$$

where ω_α is the weighting factor and has the values for the directions in D2Q9 stencil as:

$$\omega_\alpha=\begin{cases}4/9 & \text{for } \alpha=0,\\ 1/9 & \text{for } \alpha=1,2,3,4,\\ 1/36 & \text{for } \alpha=5,6,7,8.\end{cases}$$

The macroscopic density and the momentum is calculated by the formulas, respectively:

$$\rho=\sum_\alpha f_\alpha, \tag{2.7}$$

$$\rho\vec{u}=\sum_\alpha f_\alpha\vec{e}_\alpha. \tag{2.8}$$

Pressure is related with density using the isentropic relation, $p=c_s^2\rho$. The relaxation time is function of kinematic viscosity and the relation is given by $\tau=\nu/c_s^2$.

2.2 The nondimensional form

It is common practice to use nondimensional form of the governing equations in CFD. The nondimensional form of the Discrete Velocity Boltzmann Equation is obtained by

https://doi.org/10.4208/cicp.OA-2016-0014 Published online by Cambridge University Press

Table 1: Dimensional and non-dimensional forms.

	dimensional	non-dimensional
length	x	$\hat{x}=\frac{x}{L}$
time	t	$\hat{t}=\frac{tc}{L}$
velocity	$\vec{u}$	$\hat{\vec{u}}=\frac{\vec{u}}{c}$
discrete velocity	$\vec{e_\alpha}$	$\hat{\vec{e_\alpha}}=\frac{\vec{e_\alpha}}{c}$
distribution function	f_α	$\hat{f}_\alpha=\frac{f_\alpha}{\rho_\infty}$
macroscopic density	ρ	$\hat{\rho}=\frac{\rho}{\rho_\infty}$
pressure	p	$\hat{p}=\frac{P}{\rho c_s^2}$
kinematic viscosity	ν	$\hat{\nu}=\frac{\nu}{cL}$
nondimensional relaxation	τ_c	$\hat{\tau}=\frac{\tau_c}{L/c}$

choosing the variables L as the reference length, c as the reference velocity and free stream density as the reference densityρ_∞ The time used for non-dimensionalization is used as the ratio of reference length to reference velocity. The dimensional and non-dimensional quantities are given in Table 1.

By using the variables, the non-dimensional form of the discrete velocity Boltzmann equation (Eq. (2.4)) and the equilibrium distribution function (Eq. (2.6)) can be written as follows:

$$\frac{\partial \hat{f}_\alpha}{\partial \hat{t}}+\hat{\vec{e}}_\alpha\cdot\hat{\vec{\nabla}}\hat{f}_\alpha=-\frac{1}{\hat{\tau}}(\hat{f}_\alpha-\hat{f}_\alpha^{eq}), \tag{2.9}$$

$$\hat{f}_\alpha^{eq}=\hat{\rho}\omega_\alpha\left[1+3\hat{\vec{e}}_\alpha\cdot\hat{\vec{u}}+\frac{9}{2}(\hat{\vec{e}}_\alpha\cdot\hat{\vec{u}})^2-\frac{3}{2}\hat{\vec{u}}^2\right]. \tag{2.10}$$

Starting from the Reynolds number equation $Re_\infty=\frac{\rho UL}{\mu}$, relationship between the major flow parameters and the non-dimensional kinematic viscosity is obtained as follows:

$$\hat{\nu}=\frac{Ma_\infty}{\sqrt{3}Re_\infty}. \tag{2.11}$$

Ma_∞ is the Mach number of the free stream and Re_∞ is the Reynolds number depending on the reference length L and free stream velocity magnitude U_∞.

For simplicity, in the rest of the paper, the hats are omitted not used and all parameters and variables are nondimensional unless stated otherwise explicitly.

2.3 Cell centered finite volume discretization

A cell centered finite volume formulation used by Peng et al. [37], Stiebler et al. [44], Patil et al. [35] and Zarghami et al. [55] is implemented in this study. The standard Lattice

https://doi.org/10.4208/cicp.OA-2016-0014 Published online by Cambridge University Press

Boltzmann Equation is integrated over the control volume with the following assumptions:

- The equilibrium distribution function and the distribution function is assumed to be constant inside the control volume.
- The fluxes are calculated by finding the distribution function values on the boundary of the control volumes by some interpolation schemes using the neighboring cell.

The control volume with the quadrilateral elements are shown in Fig. 2.

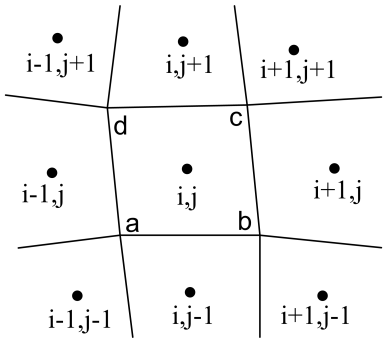


Figure 2: Quadrilateral control volume elements.

The standard discrete velocity Lattice Boltzmann Equation turns into Eq. (2.12) when integrated over a control volume. Although the implementation is 2D, derivation is assumed to be performed for a unit depth 3D element

$$\int_V \left[\frac{\partial f_\alpha}{\partial t}\right] dV + \int_V \left[\vec{e_\alpha}\cdot\vec{\nabla} f_\alpha\right] dV = \int_V \left[-\frac{1}{\tau_c}(f_\alpha - f_\alpha^{eq})\right] dV. \tag{2.12}$$

By applying the Gauss divergence theorem to the second term which is the advection of the distribution function is turned into the flux term. After performing some algebra for the quadrilateral elements used in the implementation, Eq. (2.12) can be rewritten as:

$$\frac{\partial f_\alpha}{\partial t} + \frac{1}{V}\sum_{i=1}^{\#faces} f_{\alpha,i}(\vec{n}\cdot\vec{e_\alpha})A_i = -\frac{1}{\tau_c}(f_\alpha - f_\alpha^{eq}), \tag{2.13}$$

where V is the volume of the cell, A is the face area and $\vec{n}$ is the unit vector pointing outward of the cell on the related face. The summation is performed on all faces of the control volume, in which $\#faces=4$ for the quadrilateral element for the 2D implementation. In Eq. (2.13), the distribution functions on the faces are needed to evaluate the flux term. To determine the distribution function values on faces, 2^{nd} order accurate MUSCL (Monotone Upstream centered Scheme for Conservation Laws) scheme is selected.

https://doi.org/10.4208/cicp.OA-2016-0014 Published online by Cambridge University Press

The summation of the flux integrals for each face can be collected as a single term called as numerical flux integral term F_α, which is the total transport of the distribution function through the boundaries, where

$$F_\alpha = \sum_{i=1}^{\#faces} f_{\alpha,i}(\vec{n}\cdot\vec{e_\alpha}A_i). \tag{2.14}$$

An example calculation for face (bc) of cell $[i,j]$ is shown in Eq. (2.15). The cells to be used in flux calculations are defined by the sign of the product of lattice velocity and the face normal

$$f_\alpha(bc)_{[i,j]} = \begin{cases} f_{\alpha[i,j]} + \frac{1}{4}\Big((1+\kappa)\cdot(f_{\alpha[i+1,j]} - f_{\alpha[i,j]}) \\ \qquad +(1-\kappa)\cdot(f_{\alpha[i,j]} - f_{\alpha[i-1,j]})\Big) & \text{for } \vec{e_\alpha}\cdot\vec{n}(bc)_{[i,j]} \geq 0, \\ f_{\alpha[i+1,j]} + \frac{1}{4}\Big((1+\kappa)\cdot(f_{\alpha[i,j]} - f_{\alpha[i+1,j]}) \\ \qquad +(1-\kappa)\cdot(f_{\alpha[i+1,j]} - f_{\alpha[i+2,j]})\Big) & \text{for } \vec{e_\alpha}\cdot\vec{n}(bc)_{[i,j]} < 0. \end{cases} \tag{2.15}$$

The term κ determines the spatial accuracy. A second order spatial accuracy is obtained by setting κ term to $1/3$ [4, p. 96]. Using Eq. (2.15) the second term of Eq. (2.13) for cell $[i,j]$ can be rewritten as follows:

$$\begin{aligned} F_{\alpha[i,j]} = &\left(\vec{e_\alpha}\cdot\vec{n}(ab)_{[i,j]}\right) f_\alpha(ab)_{[i,j]} A(ab)_{[i,j]} + \left(\vec{e_\alpha}\cdot\vec{n}(bc)_{[i,j]}\right) f_\alpha(bc)_{[i,j]} A(bc)_{[i,j]} \\ &+ \left(\vec{e_\alpha}\cdot\vec{n}(cd)_{[i,j]}\right) f_\alpha(cd)_{[i,j]} A(cd)_{[i,j]} + \left(\vec{e_\alpha}\cdot\vec{n}(da)_{[i,j]}\right) f_\alpha(da)_{[i,j]} A(da)_{[i,j]}. \end{aligned} \tag{2.16}$$

Eq. (2.16) collects all the flux from the surfaces under a numerical flux integral term and Eq. (2.12) is reconstructed by substituting Eq. (2.16)

$$\frac{\partial f_{\alpha[i,j]}}{\partial t} + \frac{1}{V_{[i,j]}} F_{\alpha[i,j]} = -\frac{1}{\tau_c}(f_{\alpha[i,j]} - f^{eq}_{\alpha[i,j]}). \tag{2.17}$$

2.4 Advancement in time (implicit formulation)

For the explicit solution of the D2Q9 model, 9 independent equations are solved for each discrete velocity direction for time advancement. Putting Eq. (2.17) into a new vector form given in Eq. (2.18) is the first step of implicit formulation. The $[i,j]$ index is omitted since all the terms belong to the same control volume.

$$\frac{\partial}{\partial t}\vec{f} = -\frac{1}{V}\vec{F} - \frac{1}{\tau_c}(\vec{f} - \vec{f^{eq}}), \tag{2.18}$$

https://doi.org/10.4208/cicp.OA-2016-0014 Published online by Cambridge University Press

where

$$\vec{f}=\begin{bmatrix} f_0 \\ f_1 \\ f_2 \\ f_3 \\ f_4 \\ f_5 \\ f_6 \\ f_7 \\ f_8 \end{bmatrix}, \quad \vec{f^{eq}}=\begin{bmatrix} f_0^{eq} \\ f_1^{eq} \\ f_2^{eq} \\ f_3^{eq} \\ f_4^{eq} \\ f_5^{eq} \\ f_6^{eq} \\ f_7^{eq} \\ f_8^{eq} \end{bmatrix}, \quad \vec{F}=\begin{bmatrix} F_0 \\ F_1 \\ F_2 \\ F_3 \\ F_4 \\ F_5 \\ F_6 \\ F_7 \\ F_8 \end{bmatrix}.$$

A general discretization scheme for Eq. (2.18) is given in Eq. (2.19). By setting the parameter $\beta=1$ a fully implicit backward difference method is applied

$$\frac{\vec{f}^{(n+1)}-\vec{f}^{(n)}}{\Delta t}=\beta\cdot\vec{RHS}^{(n+1)}+(1-\beta)\cdot\vec{RHS}^{(n)}. \tag{2.19}$$

In Eq. (2.19), the RHS term is equal to $-\frac{1}{V}\vec{F}-\frac{1}{\tau_c}(\vec{f}-\vec{f^{eq}})$ and is needed to be calculated at the $(n+1)^{st}$ time level where the macroscopic quantities and distribution functions are unknown. A linear approximation to the RHS of the equation can be written as follows:

$$\vec{RHS}^{(n+1)}\backsimeq\vec{RHS}^{n}+\left(\frac{\partial}{\partial\vec{f}}\vec{RHS}\right)^{(n)}\cdot\Delta\vec{f}^{(n)}, \tag{2.20}$$

where $\Delta\vec{f}^{(n)}$is defined as $\vec{f}^{(n+1)}-\vec{f}^{(n)}$. Combining Eqs. (2.19) and (2.20) and substituting the RHS into combined equation, Eq. (2.21) is obtained and it is written more explicitly in Eq. (2.22).

$$\frac{\Delta\vec{f}^{(n)}}{\Delta t}=\left[-\frac{1}{V}\vec{F}-\frac{1}{\tau_c}(\vec{f}-\vec{f^{eq}})\right]^{(n)}+\left[\frac{\partial}{\partial\vec{f}}\left(-\frac{1}{V}\vec{F}-\frac{1}{\tau_c}(\vec{f}-\vec{f^{eq}})\right)\right]^{(n)}\cdot\Delta\vec{f}^{(n)}, \tag{2.21}$$

$$\Delta\vec{f}=-\frac{\Delta t}{V}\vec{F}-\frac{\Delta t}{\tau_c}\vec{f}+\frac{\Delta t}{\tau_c}\vec{f^{eq}}+\left(-\frac{\Delta t}{V}\frac{\partial}{\partial\vec{f}}\vec{F}-\frac{\Delta t}{\tau_c}\frac{\partial}{\partial\vec{f}}\vec{f}+\frac{\Delta t}{\tau_c}\frac{\partial}{\partial\vec{f}}\vec{f^{eq}}\right)\Delta\vec{f}. \tag{2.22}$$

Since all terms of the Eq. (2.22) is at time level (n) the superscript is dropped for simplicity. Collecting the $\Delta\vec{f}$ terms in the left side Eq. (2.23) is obtained

$$\Delta\vec{f}\left[1+\underbrace{\frac{\Delta t}{\tau_c}\frac{\partial}{\partial\vec{f}}\vec{f}}_{1}-\underbrace{\frac{\Delta t}{\tau_c}\frac{\partial}{\partial\vec{f}}\vec{f^{eq}}}_{2}+\underbrace{\frac{\Delta t}{V}\frac{\partial}{\partial\vec{f}}\vec{F}}_{3}\right]=\underbrace{-\frac{\Delta t}{V}\vec{F}}_{4}\underbrace{-\frac{\Delta t}{\tau_c}\vec{f}}_{5}+\underbrace{\frac{\Delta t}{\tau_c}\vec{f^{eq}}}_{6}. \tag{2.23}$$

The terms numbered as 4 to 6 on the right hand side can be considered as the Residual term $\vec{R}$ and there is no challenge to calculate them. The term numbered as 1 includes the

https://doi.org/10.4208/cicp.OA-2016-0014 Published online by Cambridge University Press

Jacobian of the distribution function which is a 9×9 identity matrix. And the 2^{nd} term includes the Jacobian of the Equilibrium Distribution Function (JEDF) which is a non-zero 9×9 matrix. The JEDF is the link between the distribution functions of discrete directions through macroscopic quantities given in Eqs. (2.7) and (2.8). The formula of each element of the JEDF is given in Eq. (2.24) where α and β is dummy indexes. However, the term numbered as 3 includes the Jacobian of the numerical flux integral term of distribution function $\frac{\partial}{\partial \vec{f}}\vec{F}$. It is a 9×9 matrix for the D2Q9 stencil and all the non-diagonal elements are zero. The $\Delta\vec{f}$ is taken from the cell in focus or the neighboring (first order upwind) cells according to sign of the face $\vec{n}\cdot\vec{e_\alpha}$ property [4, p. 194]

$$\text{JEDF}_{\alpha,\beta}=\frac{\partial f_\alpha^{(eq)}}{\partial f_\beta}=\omega_\alpha\left[\begin{array}{c}1+3\vec{c_\alpha}\cdot\vec{u}+\frac{9}{2}(\vec{c_\alpha}\cdot\vec{u})-\frac{3}{2}(\vec{u}\cdot\vec{u})+\cdots\\(3\vec{c_\alpha}+9(\vec{c_\alpha}\cdot\vec{u})\vec{c_\alpha}-3\vec{u})\cdot(\vec{c_\beta}-\vec{u})\end{array}\right]. \tag{2.24}$$

The generic resulting system of equations for a m by n element 2D domain is given in Eq. (2.25)

$$\Big[A\Big]_{m\cdot n,m\cdot n}\Big[X\Big]_{m\cdot n}=\Big[B\Big]_{m\cdot n}, \tag{2.25}$$

where A is the square coefficient matrix also called implicit operator matrix [4, p. 195], The A matrix is a sparse matrix. X is the unknown vector and B is the residual vector. All elements of A are 9×9 submatrices, only the main diagonal, the upper and lower neighbor of the main diagonal and some distinct elements due to spatial derivatives are non zero. The shape of matrix A, vector X and vector B is shown in Fig. 3, all elements of X and B (each round shape) are 9 element column vectors of $\Delta\vec{f}$ and $\vec{R}$, respectively.

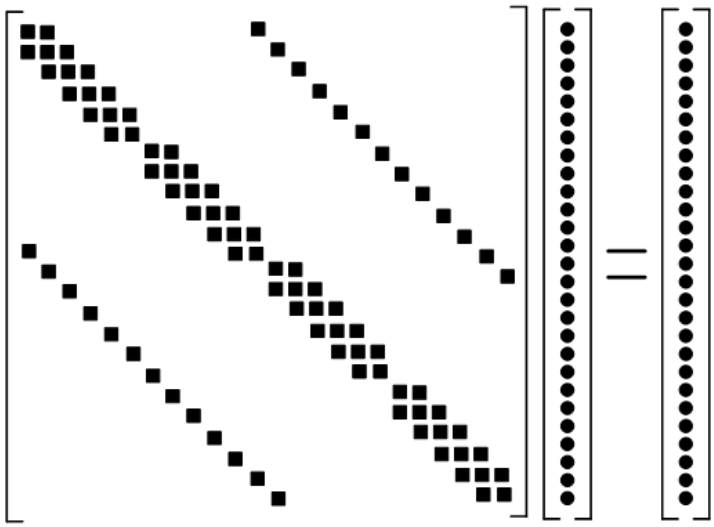


Figure 3: Implicit operator matrix.

https://doi.org/10.4208/cicp.OA-2016-0014 Published online by Cambridge University Press

The equation system is solved by using the approximate factorization method presented in Subsection 2.7. The solution is further accelerated using the local time step. Each cell uses a different time step based on the local numerical stability criterion. The details of using the local time step can be found in the work of Inamuro et al. [24].

2.5 Boundary conditions

Guo and Zheng [17] proposed an extrapolation method to implement the boundary conditions. In the proposed method the boundary conditions are defined by the known macroscopic quantities instead of the distribution functions. Further more, Guo and Zheng has also shown that the extrapolation method is second order accurate and has better numerical stability compared to the alternative methods presented in their paper for comparison.

Two level of ghost cells are used for the boundary conditions of the solution domain and appropriate macroscopic variables are set depending on the boundary condition given. The equilibrium distribution functions of the ghost cells are calculated using the macroscopic quantities and the distribution function is calculated by adding the 0^{th} order extrapolation (ghost cells use the same nonequilibrium distribution functions as the neighboring interior cells) of the non-equilibrium distribution function

$$f_\alpha(ghost) = f_\alpha^{eq}(ghost) + [f_\alpha(interior) - f_\alpha^{eq}(interior)]. \tag{2.26}$$

The term in the square brackets in Eq. (2.26) is the nonequilibrium part of the distribution function of the cells next to the boundary inside the flow domain.

2.6 Turbulence modeling

The turbulence model used in this method is the Spalart-Allmaras (SA) one equation turbulence model based on the work of the Prandtl's [49] original one-equation model. The SA turbulence model [43] given in Eq. (2.27) is the transport of the kinematic eddy viscosity $\tilde{v}$. The model is used for external aerodynamics and turbo machinery, widely. This model has been shown to give good results for adverse pressure gradients and boundary layers

$$\frac{\partial \tilde{v}}{\partial t} = M(\tilde{v}) + P(\tilde{v}) - D(\tilde{v}), \tag{2.27}$$

where

$M(\tilde{v})$	advection diffusion term
$P(\tilde{v})$	production term
$D(\tilde{v})$	destruction term

https://doi.org/10.4208/cicp.OA-2016-0014 Published online by Cambridge University Press

The advection/diffusion term, production term and destruction terms are given in Eq. (2.28)

$$\begin{aligned} M(\tilde{\nu}) &= -(\vec{u}\cdot\vec{\nabla})\tilde{\nu} + \frac{1+c_{b2}}{\sigma}\vec{\nabla}\cdot[(\nu+\tilde{\nu})\vec{\nabla}\tilde{\nu}] - \frac{c_{b2}}{\sigma}(\nu+\tilde{\nu})\vec{\nabla}^2\tilde{\nu}, \\ P(\tilde{\nu}) &= c_{b1}(1-f_{t2})\tilde{S}\tilde{\nu}, \\ D(\tilde{\nu}) &= \left[c_{w1}f_w - \frac{c_{b1}}{\kappa^2}f_{t2}\left[\frac{\tilde{\nu}}{d}\right]^2\right]. \end{aligned} \tag{2.28}$$

The parameters that are used for calculating the advection/diffusion term, production term and destruction term are given as

$$\begin{aligned} &\chi = \frac{\tilde{\nu}}{\nu'}, && S = |\omega|, \\ &f_{t2} = C_{t3}exp(-C_{t4}\chi^2), && f_{v2} = 1 - \frac{\chi}{1+\chi f_{v1}}, \\ &f_w = g\left(\frac{1+C_{w3}^6}{g^6+C_{w3}^6}\right), && f_{v1} = \frac{\chi^3}{1+\chi^3 c_{v1}^3}, \\ &\tilde{S} = S + \frac{\tilde{\nu}}{\kappa^2 d^2 f_{v2}}, && g = r + C_{w2}(r^{6-r}), \\ &r = \frac{\tilde{\nu}}{\tilde{S}\kappa^2 d^2}, \end{aligned}$$

and d is the minimum distance to the closest wall boundary, ω is the viscosity and c_{b1}, c_{b2}, σ, κ, c_{w1}, c_{w2}, c_{w3}, c_{v1}, c_{t3}, c_{t4} are the model constants.

The SA eddy viscosity parameter transport equation is also solved implicitly. The same cell centered finite volume approach is used to discretize the transport equation. The RHS is linearized with respect to $\tilde{\nu}$. The time integration of LBE and the eddy viscosity parameter is decoupled. The calculated values of macroscopic quantities are used directly in eddy viscosity parameter transport equation. That is the eddy viscosity parameter is solved after the time advancement is performed for the distribution functions. The convection terms are calculated by using 2^{nd} order accurate MUSCL scheme and the diffusion terms are calculated by using 2^{nd} order central difference scheme. The time advancement is done by the backward Euler scheme. The same approximate factorization method is used to solve the eddy viscosity parameter. The solution procedure is more simple since the eddy viscosity variable is scalar.

At the wall boundaries, the eddy-viscosity variable is set to zero. For the inflow boundaries, a ratio of laminar viscosity is used. And for the outflow boundaries the eddy viscosity variable is extrapolated using the neighbor cells inside the solution domain.

After the solution of eddy viscosity parameter is finished, the turbulent kinematic viscosity is calculated using the relation $\nu_t = f_{v1}\tilde{\nu}$. Then, the relaxation time is updated

https://doi.org/10.4208/cicp.OA-2016-0014 Published online by Cambridge University Press

with the total viscosity as

$$\tau = \frac{\nu + \nu_t}{c_s^2}.$$

2.7 Approximate factorization

There are different ways to solve the system of equations shown in Fig. 3. The first one is the direct inversion of matrix A, which takes a serious amount of computer time. However, there some approximate factorization methods like Alternating Direction Implicit (ADI), Diagonally Dominant Alternating Direction Implicit (DDADI) and Lower-Upper Symmetric Gauss Seidel (LU-SGS). A more general and comprehensive information on approximation methods are given in Refs. [25, pp. 51-59] and [4, p. 186-192].

For present implementation, ADI method is chosen. Eq. (2.23) can be turned into Eq. (2.29)

$$\left[L^I + D^I + U^I\right]\left[L^J + D^J + U^J - \frac{\Delta t}{\tau_c}\frac{\partial}{\partial \vec{f}}\vec{f}^{eq}\right]\Delta\vec{f} = \vec{R}. \tag{2.29}$$

The solution can be obtained as follows:

$$\left[L^I + D^I + U^I\right]\Delta\vec{f}^{(1)} = \vec{R},$$
$$\left[L^J + D^J + U^J - \frac{\Delta t}{\tau_c}\frac{\partial}{\partial \vec{f}}\vec{f}^{eq}\right]\Delta\vec{f} = \Delta\vec{f}^{(1)}.$$

All elements in the given matrices are matrix blocks, it is necessary to use an algorithm for block tri-diagonal systems. Two step sweeping is required to solve 2D problems. However, for the first sweep, since all the sub-matrices are diagonal, the standard Thomas Algorithm (TDMA) is sufficient to solve. For the second sweep, the JEDF adds non-zero elements to the sub matrices of D matrix. The second sweep is solved with a similar algorithm for the block tri-diagonal systems.

3 Validation of the IFVLBM

To validate the method used in this study, various flow problems are solved. The first three problems are the laminar cases, namely flow inside a lid-driven cavity, flow over a flat plate, and a circular cylinder.

3.1 Laminar steady flow

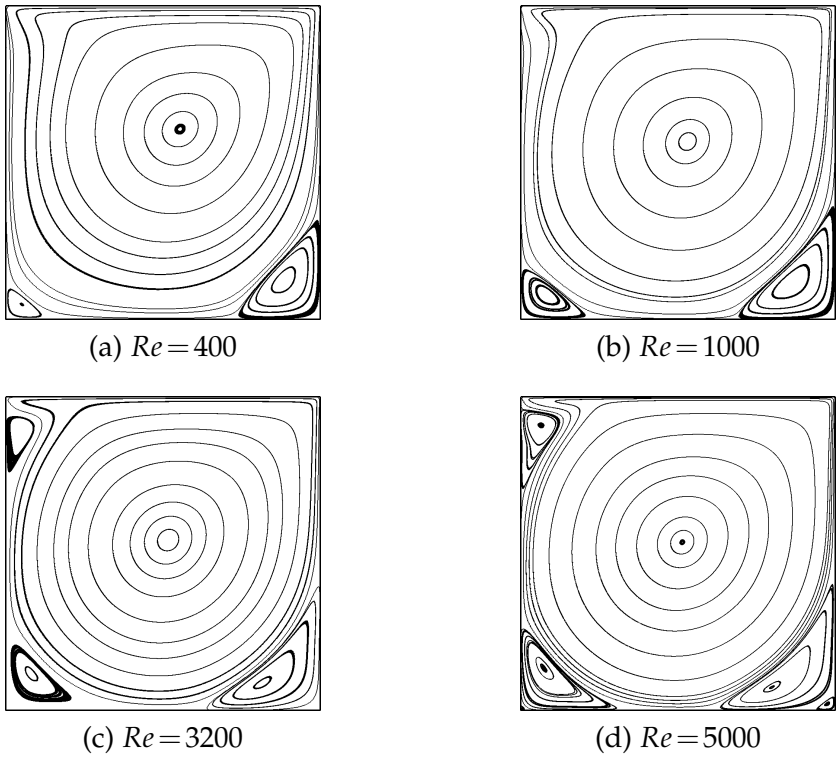
3.1.1 Lid driven cavity flow

Lid driven cavity is the one of the famous benchmarks for the CFD community. Although, it seems an easy problem, the intersection point of the stationary wall and moving wall may cause difficulties for some methods, yet must be handled carefully. The

https://doi.org/10.4208/cicp.OA-2016-0014 Published online by Cambridge University Press

calculations are done for 4 different Reynolds numbers starting from 400 to 5000. The results in the work of Ghia et al. [14] (high fidelity solution of Navier Stokes equations) are used for comparison purposes as done by many other researchers. The cavity has equal dimensions in width and height direction. The top edge is considered as a moving wall with a reference velocity from left to right. The cavity flow for the considered ranges can be categorized as a incompressible, laminar flow. The nature of the flow for Reynolds numbers 400 and 1000 is visualized as a large vortex occupying almost all the flow field accompanied by 2 small vortexes at the lower corners. For Reynolds numbers 3200 and 5000, an additional vortex at the upper left corner is formed.

The flow domain for $Re=400$, 1000 and 3200 are composed of 128 x 128 uniform cells and for $Re=5000$ 256×256 uniform cells. That is 129 x 129 grid points for the first 3 three cases and 257 x 257 for the last case as presented in Ghia et. al's work. The streamlines calculated using IFVLBM with MUSCL for the fluxes inside the cavity are presented in Fig. 4. The general arrangement of the streamlines are in a good agreement with the work of Ghia et al.. Furthermore, the center coordinates of the eddies are compared with the results of Ghia's in Table 2. The center coordinates of the eddies are also in good agreement with the Ghia's work. The secondary eddies for bottom right and bottom left positions are captured for $Re=5000$ with the present method.



(a) $Re=400$ (b) $Re=1000$

(c) $Re=3200$ (d) $Re=5000$

Figure 4: Streamlines inside the cavity obtained by IFVLBM solution data for various Reynolds numbers.

https://doi.org/10.4208/cicp.OA-2016-0014 Published online by Cambridge University Press

Table 2: Comparison of IFVLBM and center coordinates of eddies for the Eddies.

Re	Eddy	Ghia et al.		IFVLBM	
		x	y	x	y
400	PE	0.5547	0.6055	0.5543	0.6068
	BR	0.8906	0.1250	0.8830	0.1244
	BL	0.0508	0.0469	0.0517	0.0474
1000	PE	0.5313	0.5625	0.5299	0.5678
	BR	0.8594	0.1094	0.8601	0.1146
	BL	0.0859	0.0781	0.0827	0.0778
3200	PE	0.5165	0.5469	0.5161	0.5435
	BR	0.8125	0.0859	0.8149	0.0865
	BL	0.0859	0.1094	0.0803	0.1175
	TL	0.0547	0.8984	0.0549	0.8983
5000	PE	0.5117	0.5352	0.5134	0.5369
	BR1	0.8086	0.0742	0.7980	0.0748
	BL1	0.0703	0.1367	0.0720	0.1357
	BR2	0.9805	0.0195	0.9742	0.0214
	BL2	0.0117	0.0078	0.0056	0.0084
	TL	0.0625	0.9102	0.0644	0.9092

Moreover, to complete the analysis, horizontal and vertical velocity profiles are plotted at the horizontal and vertical geometrical center of the cavity. As shown in Fig. 5 and Fig. 6, the velocity profiles are matched perfectly with the reference data of Ghia et al..

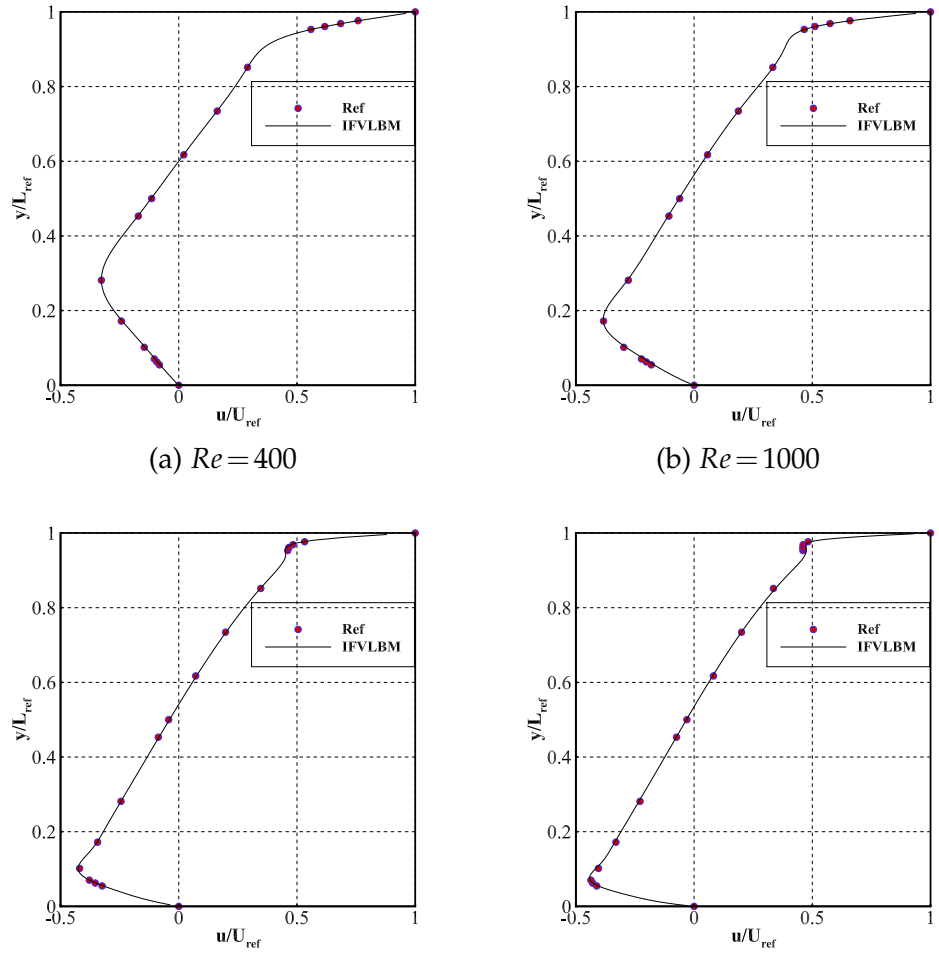
3.1.2 Steady flow past a cylinder

To demonstrate the capability and performance of the IFVLBM for more general flows, it is applied to the flow past a circular cylinder. The flow past a circular cylinder is studied both experimentally and numerically by various scientists. To compare the results obtained from the IFVLBM following studies are selected from the literature. The experimental work of Coutanceau & Bouard [8], NS solutions of F. Nieuwstadt & Keller [33], LBM solutions of He & Doolen [20] and Mei & Shyy [29]. The characteristic of the flow around a cylinder for the specified Reynolds number is the length of the eddies occurred after the cylinder, the separation point of separating streamline and drag coefficient (C_d).

The grid generated for the problem is a 201×173 nodes "O" type grid. The solutions are obtained for $Re=10, 20, 40$. The cylinder diameter is 1 unit. The first cell height from the surface of the cylinder is 0.001 diameter. The separation angle is measured from the horizontal axis where the free stream velocity is parallel. The length of the eddies referenced to the radius of the cylinder.

The length of the eddies are dependent to the Reynolds number and they are stretch-

https://doi.org/10.4208/cicp.OA-2016-0014 Published online by Cambridge University Press



(a) $Re=400$ (b) $Re=1000$

(c) $Re=3200$ (d) $Re=5000$

Figure 5: Horizontal velocity distribution at vertical geometric center-line, IFVLBM (solid lines) results from Ghia et al. (circles).

ing up to some Reynolds number around $Re \geq 50$. After that Reynolds number, the eddies are detached from the cylinder one after another periodically. The detached eddies travel to the downstream of the flow and they form a phenomena known as the Karman Vortex Street.

For laminar flow past a cylinder case, the shape of the eddies are symmetric for $Re = 10, 20, 40$. The calculated streamlines are shown in Fig. 7. The calculated values for L/r, θ and C_d are given in Table 3. The results are in very good agreement with the selected studies from the literature. Except for the separation angle for $Re = 40$, all results of IFVLBM are neither minimum nor maximum among the values obtained from the selected studies.

https://doi.org/10.4208/cicp.OA-2016-0014 Published online by Cambridge University Press

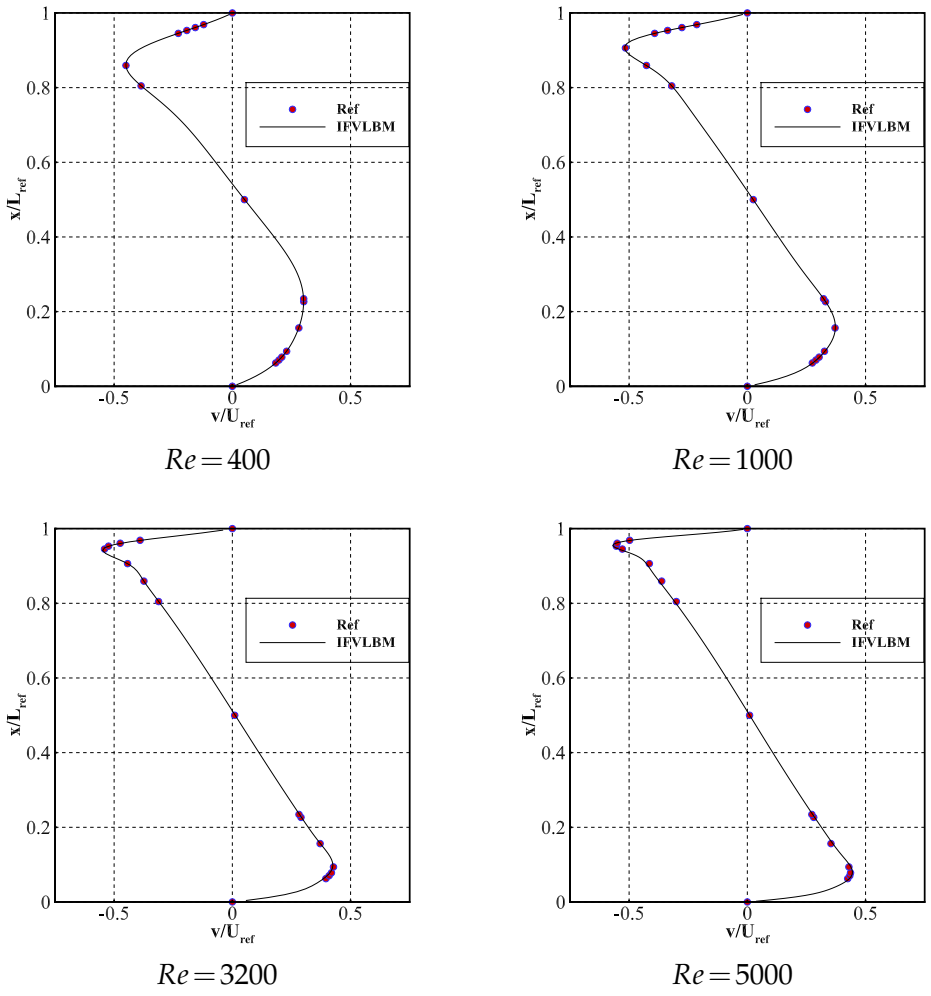


Figure 6: Vertical velocity distribution at horizontal geometric center-line, IFVLBM (solid lines) results from Ghia et al. (circles).

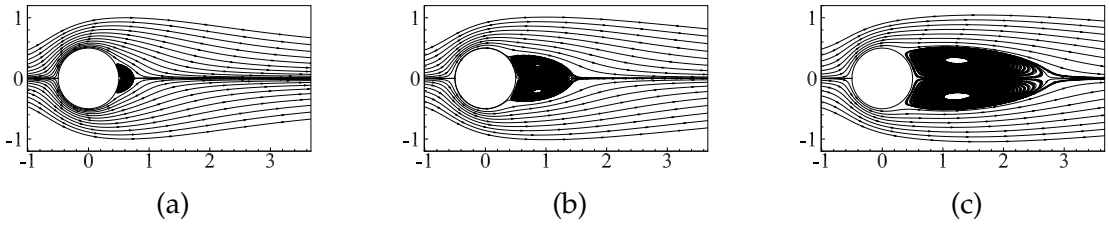


Figure 7: Some streamlines and eddy formations for the flow over cylinder for Reynolds numbers (a) $Re=10$, (b) $Re=20$, (c) $Re=40$.

https://doi.org/10.4208/cicp.OA-2016-0014 Published online by Cambridge University Press

Table 3: Characteristic parameters for flow over a cylinder.

	$Re=10$			$Re=20$			$Re=40$		
	L/r	θ	C_d	L/r	θ	C_d	L/r	θ	C_d
[33]	0.434	27.96	2.828	1.786	43.37	2.053	4.357	53.34	1.550
[8]	0.680	32.50	-	1.860	44.80	-	4.260	53.50	-
[20]	0.474	26.89	3.170	1.842	42.90	2.152	4.490	52.84	1.499
[29]	0.498	30.00	-	1.804	42.10	-	4.380	53.12	-
IFVLBM	0.486	30.05	2.962	1.853	44.05	2.084	4.425	53.77	1.544

3.1.3 Flow over a flat plate

One of the favourite test case for CFD studies is the laminar, incompressible low over a flat plate with zero pressure gradient. The problem was studied by Blassius and the solution of the nonlinear ordinary differential equation for the laminar boundary layer derived by him exits [48]. The results of Blassius' study are used to validate the present IFVLBM. The problem is set by using a H type grid including 273×193 nodes obtained from Ref. [1]. The first layer is placed at 1×10^{-6} and the length of the plate is 2 units.The studies are performed for $Re=10000$ and $Re=100000$ per unit length. The non-dimensional velocity distribution in the boundary layer region and the calculated C_f values are compared with the solution of ODE. The velocity profiles are obtained at a section placed in the middle of the flat plate.

The velocity distributions given in Fig. 8 are in good agreement with the reference solution. Moreover the friction coefficient along the flat plate is calculated and compared with the Blassius solution. The comparison for $Re=10000$ and $Re=100000$ is given in Fig. 9.

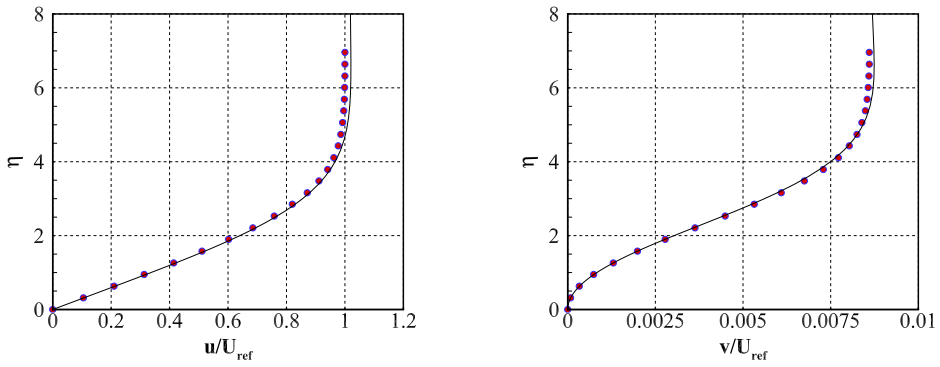
3.2 Turbulent flow

As mentioned in Turbulence Modeling section (Section 2.6), Spalart Allmaras single equation model is incorporated with the method. To validate the turbulence model, two test cases are selected. The turbulent flow over a flat plate and flow over NACA0015 are simulated. The results are presented in the following sections.

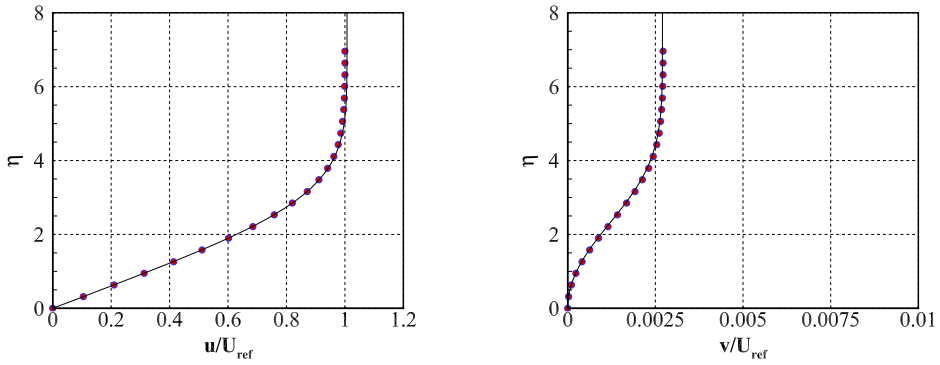
3.2.1 Flow over a flat plate

The problem is set by using a H type grid including 545×385 nodes which is obtained from the web page given in Ref. [1]. CFL3D is the structured grid, cell centered Finite Volume CFD code developed by NASA. CFL3D is a RANS solver. The grid is the same grid where the CFL3D test cases are insensitive to grid size obtained from the grid dependence studies from the same reference. The first layer is placed at 1×10^{-6} and the length of the plate is 2 units. The study is performed for $Re=5000000$ per unit length. The

https://doi.org/10.4208/cicp.OA-2016-0014 Published online by Cambridge University Press

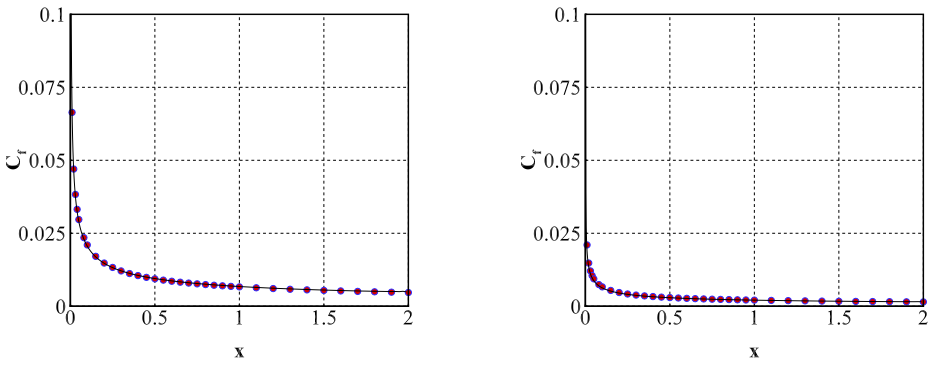


(a) $Re=10000$



(b) $Re=100000$

Figure 8: Velocity distributions in the boundary layer, the Blassius solutions are given as circles and IFVLBM solutions are given as lines, left figures are horizontal velocity components and right figures are vertical velocity components inside the boundary layer.



(a) $Re=10000$ (b) $Re=100000$

Figure 9: Friction coefficient along the flat plate, the Blassius solutions are given as circles and IFVLBM solutions are given as lines.

https://doi.org/10.4208/cicp.OA-2016-0014 Published online by Cambridge University Press

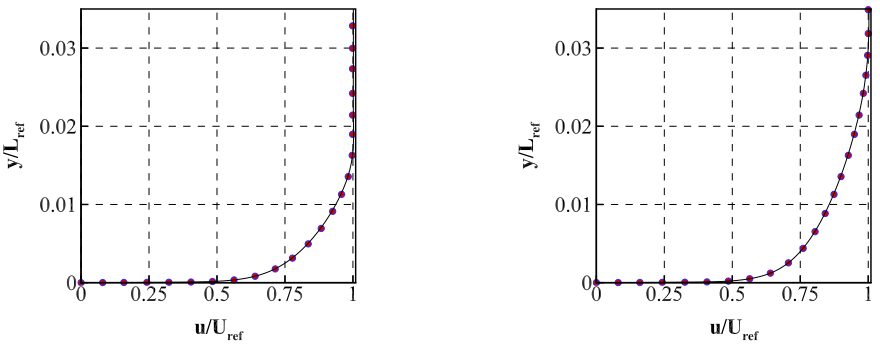


Figure 10: Velocity distributions in the boundary layer at locations $x=0.97008$ (left) and $x=1.90334$ (right) CFL3D results are given as blue circles filled with red and IFVLBM solutions are given as solid lines.

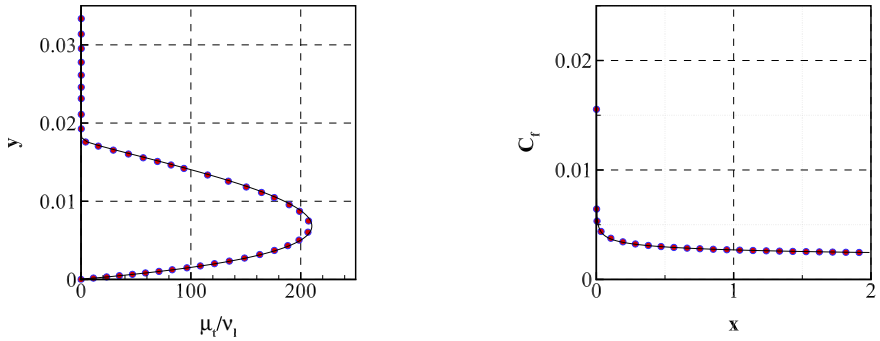


Figure 11: Ratio of turbulent viscosity to laminar viscosity at $x=0.97008$ and C_f values along the flat plate, CFL3D results are given as blue circles filled with red and IFVLBM solutions are given as solid lines.

non-dimensional velocity distribution in the boundary layer region and the calculated C_f values are compared with the results of CFL3D flat plate benchmark results.

The boundary layer velocity distributions for different x locations are given in Fig. 10. The results are in very good agreement with CFL3D code results. Actual CFL3D data is more dense but for clarity, some points are omitted.

The C_f values along the flat plate are also in perfect agreement with CFL3D. The results for the flat plate is satisfactory compared with the NASA CFL3D code.

3.2.2 Flow over NACA0015 airfoil

NACA0015 airfoil is studied excessively by Piziali [38] and the technical report has been published in 1994. The tests are conducted to identify some dynamic characteristics of the airfoil section and the 3D wing like stall. Especially the pitching motion is simulated to characterize a helicopter rotor blade. Moreover some steady state 2D data is also included in the document. A boundary layer trip is used at the leading edge during the tests.

https://doi.org/10.4208/cicp.OA-2016-0014 Published online by Cambridge University Press

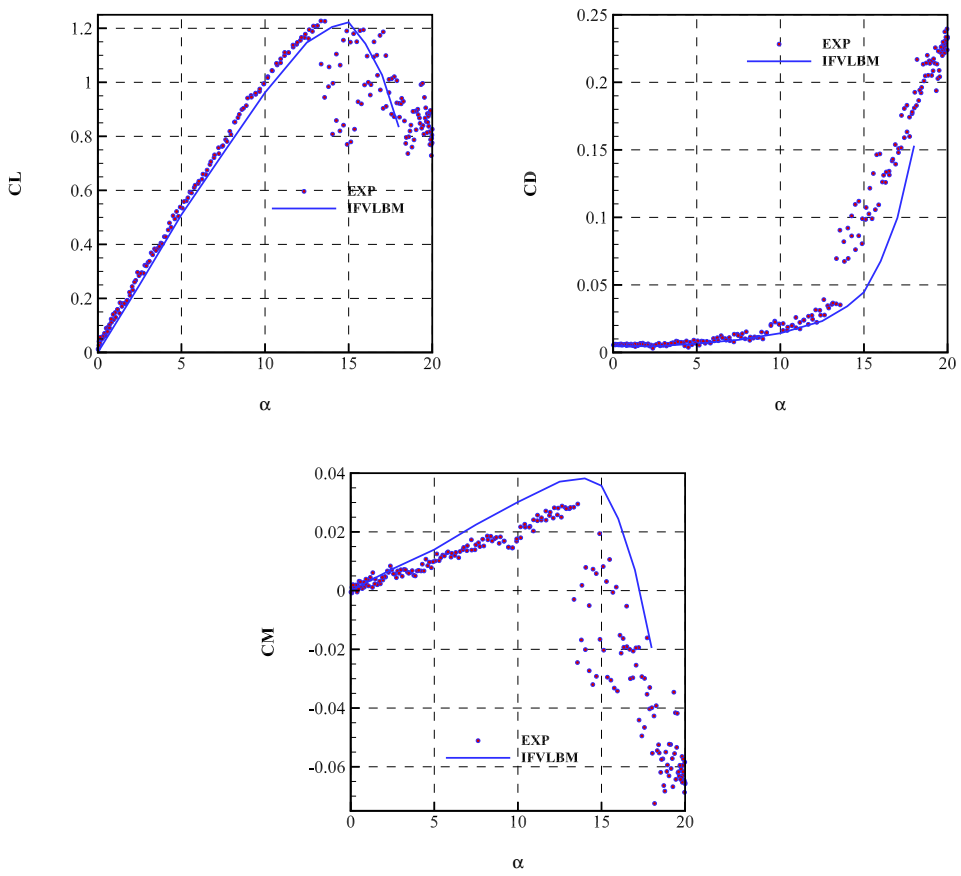


Figure 12: Static aerodynamic coefficients of NACA 0015 airfoil, the red dots with blue border are the experimental values, solid blue line is the results of IFVLBM results.

For this study NACA0015 airfoil is presented by a 377×171 C-type grid. The flow is solved as fully turbulent at $Re=1955000$. Moreover, $M=0.29$ and free stream turbulence level is 1.341946 is taken for the simulations. The angle of attacks used for the simulations are 0.0, 2.5, 5.0, 7.5, 10.0, 12.5, 15.0, 16.0 and 18.0 degrees. The coefficients CL, CD and CM are shown in Fig. 12.

As seen from Fig. 12 the results are in good agreement with the experimental results for the drag coefficient CD only the pressure drag from the simulation results are used since the drag coefficient of the experiment was calculated by using the pressure taps. One interesting characteristic of the NACA0015 airfoil section is the Trailing Edge (TE) separation starts around 10 degrees.

The evaluation of the TE separation is given in Fig. 13. The solution is the steady state results of IFVLBM. It can be seen that the TE separation starts around $AoA=10.0$ and it evolves. At $AoA=18.0$ degrees the airfoil is almost fully stalled.

https://doi.org/10.4208/cicp.OA-2016-0014 Published online by Cambridge University Press

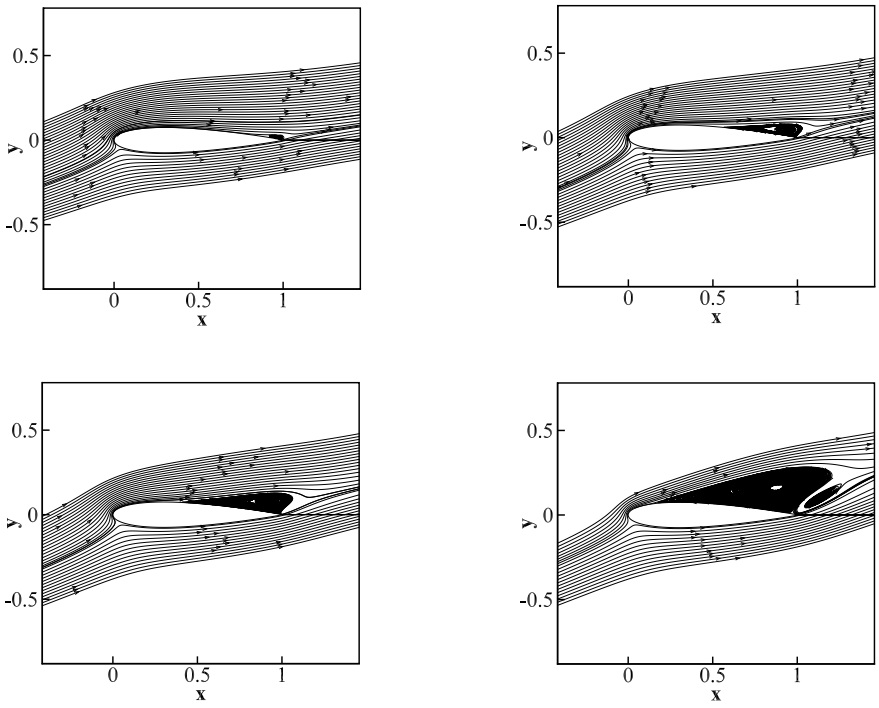


Figure 13: TE separation of NACA0015 airfoil, $AoA=10.0$ (upper left), $AoA=12.5$ (upper right), $AoA=15.0$ (lower left) and $AoA=18.0$ degrees (lower right).

3.3 Accuracy and convergence

3.3.1 Spatial accuracy

Since 2^{nd} order MUSCL scheme is used for flux calculations, IFVLBM is expected to be 2^{nd}order accurate. The accuracy of the IFVLBM is checked with the following numerical approach. The flow field solutions from different size of grid resolutions are compared with the reference solution. As the grid becomes finer, the RMS error ϵ is getting smaller. For this purpose, The solution of lid driven cavity for Re=400 from Ghia et al. [14] is used as the reference. The nondimensional u velocity values from the vertical section passing through the geometric center are used to calculate the RMS error. Calculation of the RMS error ϵ is given in Eq. (3.1). Where u is the horizontal velocity component and N is the number of spatial nodes

$$\epsilon=\sqrt{\frac{\sum(u-u_{Ghia})^2}{N^2}}. \tag{3.1}$$

After the solutions are obtained, the nondimensional u velocities at the y coordinates given in Ghia's paper are extracted. And by inspecting Eq. (3.1), it can be seen that doubling the spatial resolution, the logarithm of ϵ will be halved. Then the results is plotted

https://doi.org/10.4208/cicp.OA-2016-0014 Published online by Cambridge University Press

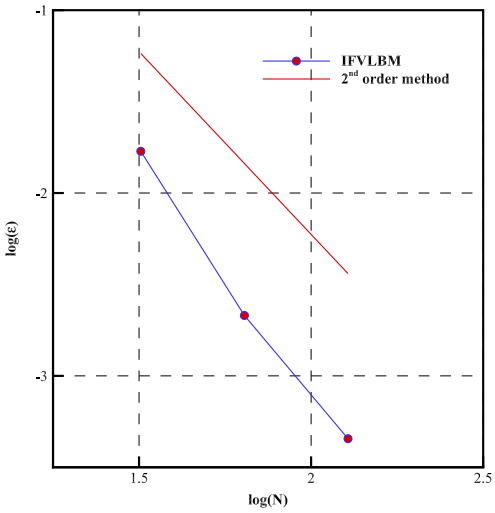


Figure 14: Numerical accuracy of IFVLBM.

against the hypothetical 2^{nd} order method for comparison in log scale for ease of understanding. As expected IFVLBM method is better than 2^{nd} order accurate hypothetical method.

3.3.2 Convergence acceleration

To assess the convergence acceleration of the proposed method, it is compared with the IMEX-LBM solution method. Guzel et al. [19]and Zarghami et al. [55] showed that using IMEX and Runge Kutta Methods the solution process becomes more stable and it can be accelerated. For the laminar cases, a solution for cavity flow on a 129×129 grid with $Re=1000$ is compared for both IMEX-LBM and IFVLBM. Both simulations are performed on a notebook computer with same compiler settings. The maximum attainable CFL number is 2.5 for IMEX-LBM and $CFL=10$ for IFVLBM without compromising the stability of the simulation. When the magnitude of density residual had reached to "-10" both simulations are stopped. In Fig. 15, it can be seen that, the simulation using IFVLBM (line with black circle symbols)is converged faster than the IMEX-LBM (dashed line with diamond symbols) despite the fact that the computational burden is more respectively.

For the turbulent case comparison, the flow over a flat plat case is used. The simulations are performed on a notebook computer. A CFL value $CFL=3.0$ for IMEX-LBM and $CFL=8.0$ for IFVLBM is used to compare the convergence acceleration. The simulations are performed for $Re=5000000$. As shown in Fig. 16, the convergence of IFVLBM (line with circle symbols) is faster than IMEX-LBM (dashed line with diamond symbols). Looking at both Figs. 15 and 16, the proposed method IFVLBM is about 2 times faster.

https://doi.org/10.4208/cicp.OA-2016-0014 Published online by Cambridge University Press

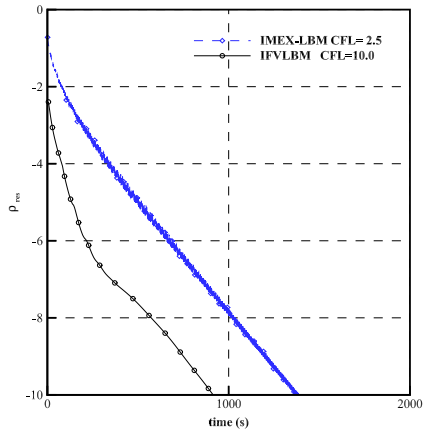


Figure 15: Convergence acceleration of IFVLBM laminar case.

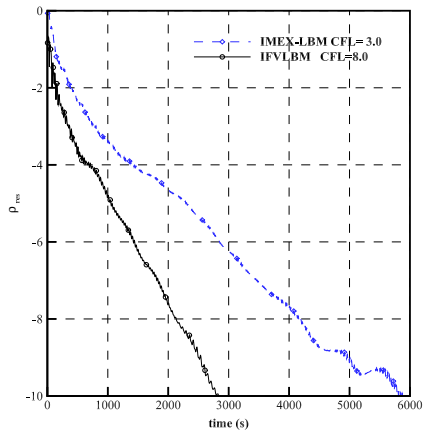


Figure 16: Convergence acceleration of IFVLBM turbulent case.

4 Conclusion and future work

The Lattice Boltzmann Method is an alternative CFD method. Scientists and researchers are trying to improve the method by applying different techniques used for the solution of the partial differential equations. The method developed in this paper is based on finite volume formulation of discrete Lattice Boltzmann Equation. Then a first order Euler-Implicit solution technique is applied to the obtained discretized equations for the Lattice Boltzmann Equation. The test cases are selected to demonstrate the laminar and turbulent capability of the presented method. The results are compared to the numerical results and experimental results presented by different researchers in the literature. All the results presented in this paper are in good agreement with the reference values.

https://doi.org/10.4208/cicp.OA-2016-0014 Published online by Cambridge University Press

In Lattice Boltzmann Methods, the values of mass and momentum in the lattice directions are related by the equilibrium distribution function. For explicit methods, it is easy to calculate the equilibrium distribution function with known quantities, however in implicit methods, after the linearization the Jacobian of the Equilibrium Distribution Function must be calculated to keep the relation of mass and momentum in the lattice directions.

For the LBM, the common practice is to use the explicit methods to exploit the parallel processing technique to increase the computing speed. At first, it seems that present method lacks the advantage of parallel processing, however when using the ADI method there are independent systems of equations for each index in the sweep direction. Each system of equation can be assigned to a core of the platform used for calculation. Then the calculation burden of the implicit methods can be traded against the increased stability and accelerated convergence.

For the future work of this study, the present method will be extended to multi-block grids and applied to 3D problems.

Acknowledgments

Authors are thankful to Mr. Guzel who supplied the Implicit Explicit Runge Kutta LBM Solutions to compare the convergence acceleration of the proposed method.

References

[1] 2d zero pressure gradient flat plate verification case. http://turbmodels.larc.nasa.gov/flatplate.html. Accessed: 2015.02.20.

[2] Uri M Ascher, Steven J Ruuth, and Raymond J Spiteri. Implicit-explicit runge-kutta methods for time-dependent partial differential equations. *Applied Numerical Mathematics*, 25(2-3):151–167, November 1997.

[3] P. L. Bhatnagar, E. P. Gross, and M. Krook. A model for collision processes in gases. i. small amplitude processes in charged and neutral one-component systems. *Phys. Rev.*, 94:511–525, May 1954.

[4] J. Blazek. *Computational Fluid Dynamics: Principles and Applications*. Elsevier, Sep 2005.

[5] Sekhar Majumdar B.N. Rajani, A. Kandasamy. Numerical simulation of laminar flow past a circular cylinder. *Applied Mathematical Modelling*, 33:1228–1247, February 2008.

[6] Nianzheng Cao, Shiyi Chen, Shi Jin, and Daniel Martinez. Physical symmetry and lattice symmetry in the lattice boltzmann method. *Phys. Rev. E*, 55:R21–R24, Jan 1997.

[7] Y. T. Chew, C. Shu, and X. D. Niu. A new differential lattice boltzmann equation and its application to simulate incompressible flows on non-uniform grids. *Journal of Statistical Physics*, 107(April):329–342, 2002.

[8] Madeleine Coutanceau and Roger Bouard. Experimental determination of the main features of the viscous flow in the wake of a circular cylinder in uniform translation. part 1. steady flow. *Journal of Fluid Mechanics*, 79:231–256, 2 1977.

https://doi.org/10.4208/cicp.OA-2016-0014 Published online by Cambridge University Press

[9] Bernd Crouse, Ernst Rank, Manfred Krafczyk, and Jonas Tölke. a lb-based approach for adaptive flow simulations. *International Journal of Modern Physics B*, 17(01n02):109–112, January 2003.
[10] H. Ding and C. Shu. A stencil adaptive algorithm for finite difference solution of incompressible viscous flows. *Journal of Computational Physics*, 214(1):397–420, 2006.
[11] Alexandre Dupuis and Bastien Chopard. Theory and applications of an alternative lattice boltzmann grid refinement algorithm. *Physical review. E, Statistical, nonlinear, and soft matter physics*, 67(6 Pt 2):066707, June 2003.
[12] O. Filippova and D. Hänel. Boundary-fitting and local grid refinement for lattice-bgk models. *International Journal of Modern Physics C*, 09:1271–1279, 1998.
[13] U. Frisch, B. Hasslacher, and Y. Pomeau. Lattice-gas automata for the navier-stokes equation. *Physical Review Letters*, 56:1505–1508, 1986.
[14] U Ghia, K.N Ghia, and C.T Shin. High-re solutions for incompressible flow using the navier-stokes equations and a multigrid method. *Journal of Computational Physics*, 48:387–411, 1982.
[15] Zhaoli Guo and Chang Shu. *Lattice Boltzmann Method and Its Applications in Engineering*. World Scientific Publishing Company, Mar 2013.
[16] Zhaoli Guo and T S Zhao. Explicit finite-difference lattice boltzmann method for curvilinear coordinates. *Physical review. E, Statistical, nonlinear, and soft matter physics*, 67(April):066709, 2003.
[17] Zhaoli Guo, Chuguang Zheng, and Baochang Shi. An extrapolation method for boundary conditions in lattice boltzmann method. *Physics of Fluids*, 14(6):2007–2010, 2002.
[18] Zhaoli Guo, Chuguang Zheng, and Baochang Shi. Domain-decomposition technique in lattice boltzmann method. *International Journal of Modern Physics B*, 17(01n02):129–133, January 2003.
[19] Goktan Guzel and Ilteris Koc. Simulation of turbulent flows using a finite-volume based lattice boltzmann flow solver. *Communications in Computational Physics*, 17:213–232, 1 2015.
[20] X He and G D Doolen. Lattice-boltzmann method on curvilinear coordinates system: flow around a circular cylinder. *Journal of Computational Physics*, 134:306–315, 1997.
[21] Xiaoyi He and Li-Shi Luo. Lattice boltzmann model for the incompressible navier stokes equation. *Journal of Statistical Physics*, 88:927–944, 1997.
[22] Xiaoyi He, Li-Shi Luo, and Micah Dembo. Some progress in lattice boltzmann method. part i. nonuniform mesh grids. *Journal of Computational Physics*, 129:357–363, 1996.
[23] Xiaoyi He, Li-Shi Luo, and Micah Dembo. Some progress in the lattice boltzmann method: Reynolds number enhancement in simulations. *Physica A: Statistical Mechanics and its Applications*, 239(13):276 – 285, 1997.
[24] Taro Imamura, Kojiro Suzuki, Takashi Nakamura, and Masahiro Yoshida. Acceleration of steady-state lattice boltzmann simulations on non-uniform mesh using local time step method. *Journal of Computational Physics*, 202:645–663, 2005.
[25] D. Kwak, C. C. Kiris *Computation of Viscous Incompressible Flows.* Springer,2011.
[26] Taehun Lee and Ching-Long Lin. A characteristic galerkin method for discrete boltzmann equation. *Journal of Computational Physics*, 171(1):336 – 356, 2001.
[27] Yusong Li, Eugene J. LeBoeuf, and P. K. Basu. Least-squares finite-element lattice boltzmann method. *Physical Review E - Statistical, Nonlinear, and Soft Matter Physics*, 69(6 2):1–4, 2004.
[28] Guy R. McNamara and Gianluigi Zanetti. Use of the boltzmann equation to simulate lattice-gas automata. *Physical Review Letters*, 61(20):2332–2335, 1988.
[29] Renwei Mei and Wei Shyy. On the finite difference-based lattice boltzmann method in curvilinear coordinate. *Journal of Computational Physics*, 143:426–448, 1998.

https://doi.org/10.4208/cicp.OA-2016-0014 Published online by Cambridge University Press

[30] Misun Min and Taehun Lee. A spectral-element discontinuous galerkin lattice boltzmann method for nearly incompressible flows. *Journal of Computational Physics*, 230(1):245–259, 2011.
[31] S. Mittal. Excitation of shear layer instability in flow past a cylinder at low reynolds number. *International Journal for Numerical Methods in Fluids*, 49(10):1147–1167, 2005.
[32] Francesca Nannelli and Sauro Succi. The lattice boltzmann equation on irregular lattices. *Journal of Statistical Physics*, 68(3-4):401–407, 1992.
[33] F. Nieuwstadt and H.B. Keller. Viscous flow past circular cylinders. *Computers & Fluids*, 1(1):59 – 71, 1973.
[34] X.D. Niu, Y.T. Chew, and C. Shu. Simulation of flows around an impulsively started circular cylinder by taylor series expansion- and least squares-based lattice boltzmann method. *Journal of Computational Physics*, 188(1):176 – 193, 2003.
[35] D. V. Patil and K. N. Lakshmisha. Finite volume tvd formulation of lattice boltzmann simulation on unstructured mesh. *Journal of Computational Physics*, 228:5262–5279, August 2009.
[36] Gongwen Peng, Haowen Xi, Comer Duncan, and So-Hsiang Chou. Lattice boltzmann method on irregular meshes. *Physical Review E*, 58(4):R4124, 1998.
[37] Gongwen Peng, Haowen Xi, Comer Duncan, and So-Hsiang Chou. Finite volume scheme for the lattice boltzmann method on unstructured meshes. *Physical Review E*, 59(4):4675, 1999.
[38] R. A. Piziali. 2-d and 3-d oscillating wing aerodynamics for a range of angles of attack including stall. NASA Technical Memorandum 4362, NASA, September 1994.
[39] O. Posdziech and R. Grundmann. A systematic approach to the numerical calculation of fundamental quantities of the two-dimensional flow over a circular cylinder. *Journal of Fluids and Structures*, 23:479–499, April 2007.
[40] A. K. Dhiman Ravi Golani. Fluid flow and heat transfer across a circular cylinder in the unsteady flow regime. *The International Journal Of Engineering And Science*, 3(3):08–19, 2014.
[41] C. Shu, Y. T. Chew, and X. D. Niu. Least-squares-based lattice boltzmann method: A meshless approach for simulation of flows with complex geometry. *Phys. Rev. E*, 64:045701, Sep 2001.
[42] C. Shu, X. D. Niu, and Y. T. Chew. Taylor-series expansion and least-squares-based lattice boltzmann method: Two-dimensional formulation and its applications. *Phys. Rev. E*, 65:036708, Mar 2002.
[43] S. R. Spalart, P.R., Allmaras, P R Spalart, and S R Allmaras. sa.pdf. AIAA Pap. 92–0439, Reno, NV, January 1992.
[44] Maik Stiebler, Jonas Tlke, and Manfred Krafczyk. An upwind discretization scheme for the finite volume lattice boltzmann method. *Computers & Fluids*, 35(8-9):814–819, 2006. Proceedings of the First International Conference for Mesoscopic Methods in Engineering and Science.
[45] Jonas Tölke, Sören Freudiger, and Manfred Krafczyk. An adaptive scheme using hierarchical grids for lattice boltzmann multi-phase flow simulations. *Computers & Fluids*, 35(8-9):820–830, September 2006.
[46] Stefano Ubertini and Sauro Succi. Recent advances of lattice boltzmann techniques on unstructured grids. *Progress in Computational Fluid Dynamics, an International Journal*, 5(1):85–96, January 2005.
[47] Y. Wang, Y. L. He, T. S. Zhao, G. H. Tang, and W. Q. Tao. Implicit-explicit finite-difference lattice boltzmann method for compressible flows. *International Journal of Modern Physics C*, 18(12):1961–1983, 2007.

https://doi.org/10.4208/cicp.OA-2016-0014 Published online by Cambridge University Press

[48] Frank White. *Viscous Fluid Flow (Mcgraw Hill Series in Mechanical Engineering)*. McGraw-Hill Science/Engineering/Math, 2005.
[49] David C. Wilcox. *Turbulence Modeling for CFD*. DCW Industries, Jan 2006.
[50] J. Wu and C. Shu. A solution-adaptive lattice boltzmann method for two-dimensional incompressible viscous flows. *Journal of Computational Physics*, 230(6):2246–2269, 2011.
[51] H Xi, G Peng, and S H Chou. Finite-volume lattice boltzmann method. *Physical Review Ew E*, 59(5):6202–6205, 1999.
[52] H Xi, G Peng, and S H Chou. Finite-volume lattice boltzmann schemes in two and three dimensions. *Physical review. E, Statistical physics, plasmas, fluids, and related interdisciplinary topics*, 60(3):3380–3388, 1999.
[53] Dazhi Yu, Dazhi Yu, Renwei Mei, Renwei Mei, Wei Shyy, and Wei Shyy. A multi-block lattice boltzmann method for viscous fluid flows. *International Journal for Numerical Methods in Fluids*, 39(October 2001):99–120, 2002.
[54] Zhao Yu and Liang-Shih Fan. An interaction potential based lattice boltzmann method with adaptive mesh refinement (amr) for two-phase flow simulation. *Journal of Computational Physics*, 228(17):6456–6478, 2009.
[55] A. Zarghami, M. J. Maghrebi, J. Ghasemi, and S. Ubertini. Lattice boltzmann finite volume formulation with improved stability. *Communications in Computational Physics*, 12(1):42–64, 2012.

https://doi.org/10.4208/cicp.OA-2016-0014 Published online by Cambridge University Press